

Unusual hyperfine interaction of Dirac electrons and NMR spectroscopy in graphene

Balázs Dóra¹ and Ferenc Simon²

¹*Max-Planck-Institut für Physik Komplexer Systeme, Nöthnitzer Str. 38, 01187 Dresden, Germany*

²*Budapest University of Technology and Economics,
Institute of Physics and Solids in Magnetic Fields Research Group,
Hungarian Academy of Sciences, P.O. Box 91, H-1521 Budapest, Hungary*

(Dated: November 1, 2018)

Theory of nuclear magnetic resonance (NMR) in graphene is presented. The canonical form of the electron-nucleus hyperfine interaction is strongly modified by the linear electronic dispersion. The NMR shift and spin-lattice relaxation time are calculated as function of temperature, chemical potential, and magnetic field and three distinct regimes are identified: Fermi-, Dirac-gas, and extreme quantum limit behaviors. A critical spectrometer assessment shows that NMR is within reach for fully ¹³C enriched graphene of reasonable size.

PACS numbers: 76.60.-k, 71.20.Tx, 85.75.-d

Nuclear magnetic resonance (NMR) is a powerful spectroscopic tool [1] and an architecture for quantum information processing [2, 3] at the same time. Both of these applications are possible due to the relatively weak interaction of the nucleus with its environment. This weak interaction is sufficient to probe the electronic state of its vicinity, which yields information about the local electron bonds or about the correlated behavior of electrons as e.g. in superconductors [4]. NMR quantum computing exploits that the nuclei are well isolated from the environment thus there is a longer time window for the manipulation and detection of the nuclear quantum state.

For both kinds of applications, the important NMR parameters are the shift of the NMR resonance with respect to a standard, and the decay of the longitudinal magnetization to its equilibrium value, the spin-lattice relaxation time, T_1 . These were extensively studied in solid state systems both theoretically and experimentally [1, 5]. However, the body of NMR experiments were focused on three-dimensional systems which stemmed from the unavailability of stable, inherently two-dimensional materials. The discovery of graphene, a single stable sheet of carbon atoms in a hexagonal lattice [6], enables studies of an exactly two-dimensional system. Its quasi-particles follow a linear band dispersion, causing the electrons to behave as massless Dirac fermions, which gives rise to unique transport and magnetic properties [7]. Similarly, unusual electron-nuclear interaction is expected.

In a metal, the NMR measurables are most affected by the surrounding electrons through the electron-nuclear hyperfine interaction (HFI). The standard, text-book form of the HFI of nuclei and conduction electrons leads to the Hamiltonian $H_{\text{HFI}} = H_{\text{orb}} + H_{\text{spin}}$ [5]:

$$H_{\text{orb}} = \frac{\mu_0}{4\pi} g \mu_{\text{B}}^* \gamma_n \mathbf{I} \frac{\mathbf{r} \times \mathbf{p}}{r^3},$$

$$H_{\text{spin}} = \frac{\mu_0}{4\pi} g \mu_{\text{B}} \hbar \gamma_n \mathbf{I} \left(\frac{\mathbf{S} r^2 - 3 \mathbf{r}(\mathbf{S} \cdot \mathbf{r})}{r^5} - \frac{8\pi}{3} \mathbf{S} \delta(\mathbf{r}) \right) \quad (1)$$

Here, the first term (H_{orb}) is due to the electron orbital

magnetism, the second (H_{spin}) contains the electron spin-dipole interaction and the so-called Fermi-contact interaction. μ_0 is the permeability of free space, γ_n is the nuclear gyromagnetic ratio, \mathbf{I} is the nuclear spin, $g \approx 2$ is the g-factor of the electrons. \mathbf{S} , \mathbf{p} , and \mathbf{r} are the electron spin, momentum, and vector operators. μ_{B} is the Bohr magneton and $\mu_{\text{B}}^* = m/m^* \mu_{\text{B}}$ is the effective orbital Bohr magneton [8], where m^* is the effective band mass and m is the mass of a free electron.

At first, it is not obvious how to generalize the orbital term of the HFI to massless Dirac fermions and its derivation is one of the primary goals of this work. Second, the unique properties of the conduction electrons of graphene are expected to give rise to unique relaxation and NMR shift behaviors. E.g. deviation from the Korringa relation [1], that is an important benchmark of non Fermi-liquid behavior, is expected.

Here, we show that the canonical description of the hyperfine interaction is modified for the massless Dirac fermions and we derive the hyperfine Hamiltonian paying special attention to obtain the appropriate orbital contribution. We identify different regimes based on the NMR measurables; Fermi-, Dirac-gas, and extreme quantum limit behaviors. We also discuss the feasibility of bulk NMR spectroscopy on graphene with a critical evaluation of NMR spectrometer performance.

The low energy excitations in graphene are described by the two-dimensional Dirac equation [7]:

$$H = v_{\text{F}}(\sigma_x p_x + \sigma_y p_y), \quad (2)$$

where $v_{\text{F}} \approx 10^6$ m/s is the Fermi velocity of graphene, and the pseudospin variables (Pauli matrices, σ) spring from the two-sublattice structure. The HFI in graphene is derived following Abragam [5] by treating the nucleus as a magnetic dipole with $\mathbf{m} = \hbar \gamma_n \mathbf{I}$. Its vector potential, $\mathbf{A}(\mathbf{r}) = \frac{\mu_0}{4\pi} \frac{\mathbf{m} \times \mathbf{r}}{r^3}$, is inserted into the kinetic momentum as $\mathbf{p} \rightarrow \mathbf{p} + e\mathbf{A}$ in addition to the electron and nuclear Zeeman terms. This calculation gives the effective HFI Hamiltonian in graphene as

$$H_{\text{HFI}}^{\text{gr}} = \frac{\mu_0}{4\pi} \hbar \gamma_n I_z \left(\frac{\mathbf{r} \times \mathbf{j}}{r^3} \right)_z + H_{\text{spin}}, \quad (3)$$

where $\mathbf{j} = ev_{\text{F}} \boldsymbol{\sigma}$ is the electric current operator in graphene and $\boldsymbol{\sigma}$ is a vector of the Pauli matrices. The first term describes the interaction of the nucleus with the orbital motion of the Dirac electrons[9], which contains I_z only as the electrons are confined in the plane. The spin-dipole and Fermi-contact terms are unchanged with respect to their usual forms.

The orbital term in Eq. (3) differs significantly from the usual form in Eq. (1) as the orbital magnetic moment ($\mathbf{r} \times \mathbf{j}$) replaces the usual term ($\frac{g\mu_{\text{B}}}{\hbar} \mathbf{r} \times \mathbf{p}$). This is the result of the peculiar form of the current operator for Dirac electrons $\mathbf{j} \sim \boldsymbol{\sigma}$, which is also responsible for the jittery motion of the center of mass coordinate known as Zitterbewegung [10]. Eq. (1) can be deduced formally from Eq. (3) by using $\mathbf{j} = e\mathbf{p}/m^*$ for a normal metal.

A unique property of the orbital magnetic moment of graphene is that it remains invariant in an applied magnetic or gauge field, since \mathbf{j} is insensitive to the vector potential. We mention that the proper orbital angular momentum of Dirac particles is still $\mathbf{r} \times \mathbf{p}$ in the sense that it is responsible for rotations in the $x - y$ plane, which differs from the orbital magnetization. We also note that there are no higher order terms in the vector potential in the graphene HFI Hamiltonian due to the linearity of the Dirac equation.

The second quantized form of the orbital part of the interaction in graphene is obtained as

$$H_{\text{orb}}^{\text{gr}} = \frac{J_{\text{orb}}}{N} I_z \sum_{\mathbf{k}\mathbf{k}'\alpha\alpha's} f(\mathbf{k}, \mathbf{k}', \alpha, \alpha') c_{\mathbf{k}\alpha s}^+ c_{\mathbf{k}'\alpha's}, \quad (4)$$

where $J_{\text{orb}} = \mu_0 \hbar \gamma_n ev_{\text{F}} / 2A_c$, and $f(\mathbf{k}, \mathbf{k}', \alpha, \alpha') = (\alpha\alpha' - \exp[i(\varphi_{\mathbf{k}} - \varphi_{\mathbf{k}'})]) (\alpha k + \alpha' k') / 2|\mathbf{k} - \mathbf{k}'|$, and $c_{\mathbf{k}\alpha s}^+$ creates a quasi-particle with energy $E_{\alpha}(\mathbf{k})$ and real spin s , $\varphi_{\mathbf{k}}$ is the angle of \mathbf{k} with the k_x axis, A_c is the unit cell area, and N is the number of unit cells. The interaction is bounded as $|f(\mathbf{k}, \mathbf{k}', \alpha, \alpha')| \leq 1$. The magnitude of the orbital term is estimated as $J_{\text{orb}} \approx 21$ MHz using $\gamma(^{13}\text{C})/2\pi = 10.7$ MHz/T.

The effective interaction describing the hyperfine interaction in graphene is obtained from Eq. 3. as

$$H_{\text{HFI}}^{\text{gr}} = \bar{\mathbf{S}}\mathbf{A}\mathbf{I} + H_{\text{orb}}^{\text{gr}}, \quad (5)$$

where $\bar{\mathbf{A}}$ is a 3x3 tensor with diagonal elements. Of these, the traceless ones are due to the spin-dipole interaction as $A_{\text{dip}}(x, y) : A_{\text{dip}}(z) = -A_{\text{dip}} : 2A_{\text{dip}}$ and the scalar term, A_{iso} , is given by the isotropic Fermi-contact interaction. First principles calculations [11] gave $A_{\text{dip}} = 73$ MHz and $A_{\text{iso}} = -44$ MHz, which gives $(-117, -117, 102)$ MHz for the diagonal elements of $\bar{\mathbf{A}}$. We note that the first principles value of A_{dip} agrees well with the $A_{\text{dip}} = 91$ MHz

obtained for the p_z orbital of a free carbon atom [1, 12], which confirms that it is indeed the relevant orbital in graphene.

Upon establishing the hyperfine interaction in graphene, we turn to the calculation of the NMR measurables. For a given magnetic field, terms of Eq. 5. perpendicular and parallel to the field contribute to relaxation and to the Knight shift, respectively [5, 13]. The spin-lattice relaxation rate, $1/T_1$ and the Knight shift, K , for a given magnetic field direction ($i = x, y, z$) are [14]

$$\left(\frac{1}{T_1 T} \right)_i = \frac{C_i^2 \pi k_{\text{B}}}{\hbar} \int_{-\infty}^{\infty} \frac{\rho(E)^2 dE}{4k_{\text{B}} T \cosh^2[(E - \mu)/2k_{\text{B}} T]}, \quad (6a)$$

$$K_i = \frac{A_i \gamma_e}{2\gamma_n} \int_{-\infty}^{\infty} \frac{\rho(E) dE}{4k_{\text{B}} T \cosh^2[(E - \mu)/2k_{\text{B}} T]}, \quad (6b)$$

with $C_i^2 = \sum_{\nu \neq i} (A_{\nu}^2/2 + \delta_{\nu,z} 2J_{\text{orb}}^2)$, γ_e is the gyromagnetic ratio of electrons, $\rho(E)$ is the quasi-particle density of states (DOS), and μ is the chemical potential. T_1 and K for an arbitrary field direction is readily obtained by angular dependent combinations [13].

The orbital interaction involves only I_z , thus it affects T_1 only when the field is in the graphene plane ($i = x, y$), which explains the $2J_{\text{orb}}^2$ term (the factor 2 comes from the spin degeneracy). The orbital term does not contribute to the Knight shift even for a magnetic field along z in a manner analogous to demagnetization. The spin part of the HFI contributes to a $\sim 15\%$ anisotropy of T_1 for in and out of plane magnetic fields but the orbital term makes it nearly isotropic. More accurate statements require the first principles calculation [11] of J_{orb} . The Knight shift changes sign and drops by 15% from in plane to out of plane fields. We omit the i index from C_i in the following.

We distinguish two scenarios for the DOS in the following calculation: (i) absence of Landau levels and (ii) where the presence of Landau levels is important. Scenario (i) occurs for three cases: when magnetic field is in the plane, when magnetic field is arbitrary but level broadening due to Γ or T makes the Landau levels undistinguishable around μ (the criterion is $v_{\text{F}}^2 e B \mu \leq \max(\Gamma, k_{\text{B}} T)$), or in the vicinity of the DP point (i.e. μ is small) when the lowest Landau level is significantly broadened due Γ or T (the criterion is $v_{\text{F}} \sqrt{2eB\hbar} \leq \max(\Gamma, k_{\text{B}} T)$).

For scenario (i), the magnetic field-free DOS can be used in the calculation and it reads as:

$$\rho(E) = \frac{A_c |E|}{2\pi \hbar^2 v_{\text{F}}^2} \quad (7)$$

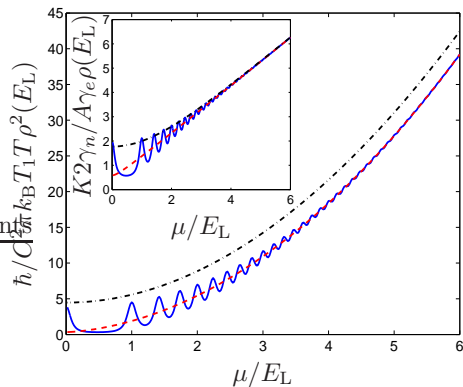


FIG. 1: (Color online) The nuclear spin relaxation rate (main figure) and the Knight shift (inset) are shown with $\Gamma = 0.1 E_L$ and $D = 1000 E_L$ as a function of the chemical potential. The blue solid/red dashed line refers to the presence/absence of magnetic field at $T = 0$, the black dash-dotted line corresponds to $k_B T = E_L$ in the presence of magnetic field. Increasing μ or T makes the Landau level structure disappear, and scenario (ii) is replaced by scenario (i).

per spin and C atom. The resulting relaxation rate is

$$\left(\frac{1}{T_1 T}\right) = C^2 \frac{\pi k_B}{\hbar} \left[\rho^2(\mu) + \rho^2\left(\frac{\pi k_B T}{\sqrt{3}}\right) \right], \quad (8)$$

which increases as $\max(\mu^2, (\pi k_B T)^2/3)$. Away from the Dirac point, μ dominates, and the temperature becomes important only near the DP.

Exactly at the DP, T_1 diverges as $T_1 \sim T^{-3}$, therefore the nuclear spins are not relaxed by conduction electrons at $T = 0$ due to the absence of charge carriers at the charge neutrality point. In the presence of impurities, the DOS at the DP reads as [15]

$$\rho(0) = \frac{A_c}{2\pi\hbar^2 v_F^2} \frac{2\Gamma}{\pi} \ln\left(\frac{D}{\Gamma}\right) \quad (9)$$

with Γ the scattering rate and D the cutoff in the continuum theory. Therefore, the aforementioned divergence of the clean system weakens to $T_1 \sim (\Gamma^2 \ln^2(D/\Gamma)T)^{-1}$, reproducing the Fermi-gas behavior. Since the DOS is finite at the DP due to impurities, the Dirac nature of the quasi-particles is lost at this level.

The Knight shift is evaluated as

$$K = A \frac{\gamma_e}{2\gamma_n} \rho \left(2k_B T \ln \left[2 \cosh \left(\frac{\mu}{2k_B T} \right) \right] \right). \quad (10)$$

It can be approximated by $K \sim \max(2k_B T \ln 2, |\mu|)$. Impurities provide a finite DOS even at the DP, therefore the Knight shift stays finite there as $K \sim \Gamma \ln(D/\Gamma)$.

Concluding scenario (i), we give $1/T_1 T$ for the case of chemical doping of, or chemisorption on the graphene layer. E.g. for an AC_x composition, where A is an alkali atom with full charge transfer, there is an extra $2/xA_c$ electron density to each lattice site. This translates to

a chemical potential shift of $\mu = \hbar v_F \sqrt{2\pi/xA_c}$, which leads to a relaxation rate as

$$\left(\frac{1}{T_1 T}\right) = \frac{k_B C^2 A_c}{2\hbar^3 v_F^2 x} \approx \frac{0.002}{x} [(\text{Ks})^{-1}], \quad (11)$$

or $T_1 \approx 500 (\text{sK}) \cdot x/T$. This gives $T_1 \approx 10$ s at 300 K for $x=8$, that is a usual doping level for graphite [16]. It shows the sensitivity of the NMR properties for doping or chemisorption, which may lead to a sensor application of graphene. The chemical potential can be also tuned by gate voltage with a less dramatic effect on T_1 .

For scenario (ii), Landau level formation is important, and the continuous spectrum is replaced by discrete Landau levels as $E_{n\alpha} = \alpha E_L \sqrt{n}$ where $\alpha = \pm$, n is non-negative integer, $E_L = v_F \sqrt{2\hbar e B_z}$ is the Landau scale, and B_z is the perpendicular component of the magnetic field. With this, the DOS reads as [15]

$$\rho(E) = \frac{A_c}{2\pi\hbar^2 v_F^2} \frac{1}{2\pi} \left[\frac{\Gamma E_L^2}{E^2 + \Gamma^2} - 4\Gamma \ln\left(\frac{E_L}{D}\right) - 2\text{Im} \left\{ (E + i\Gamma) \Psi \left(1 - \frac{(E + i\Gamma)^2}{E_L^2} \right) \right\} \right], \quad (12)$$

where $\Psi(x)$ is Euler's digamma function, and reduces to Eq. (7) for clean systems with vanishing magnetic field. The $1/T_1 T$ and the Knight shift are shown in Fig. 1 separately as a function of the chemical potential. These display the characteristic de Haas-van Alphen like oscillatory behavior at high magnetic field and low μ and T , that we refer to as the extreme quantum limit (EQL).

Calculation of the relaxation rate and Knight shift allows to test the validity of the Korringa relation, i.e. whether $1/T_1 T K^2 = \text{const.}$ holds. In general, the Korringa relation is valid for a Fermi-liquid. In particular for a non-interacting Fermi-gas [22] $(1/T_1 T K^2)_F = 4\pi k_B (\gamma_n/\gamma_e)^2/\hbar$. For graphene within scenario (i) and in the limit of $(\mu, k_B T) \gg \Gamma$, which is referred to as the scaling limit, it reads as

$$\frac{1}{T_1 T K^2} = \frac{4\pi k_B}{\hbar} \left(\frac{\gamma_n}{\gamma_e} \right)^2 \left(\frac{C^2}{A^2} \right) F \left(\frac{\mu}{k_B T} \right), \quad (13)$$

which depends only on the ratio of μ and T , and $F(x)$ is a universal scaling function

$$F(x) = \frac{3x^2 + \pi^2}{12 \ln^2[2 \cosh(x/2)]}, \quad (14)$$

which is even in x and satisfies $F(0) = \pi^2/3 \ln^2(4) \approx 1.71$ and $F(\infty) = 1$, and is shown in Fig. 2. For in-plane field, $C^2/A^2 < 1$, while for perpendicular field $C^2/A^2 > 1$. For $\mu \gg k_B T$, the DOS is finite, and nothing distinguishes graphene from a conventional metal because only one branch of the "V"-shaped dispersion is seen due to the smallness of T , therefore the usual Korringa relation is satisfied. In the opposite limit, $(\mu \ll k_B T)$, the Korringa relation leads to a constant, $F(0)$, times bigger than

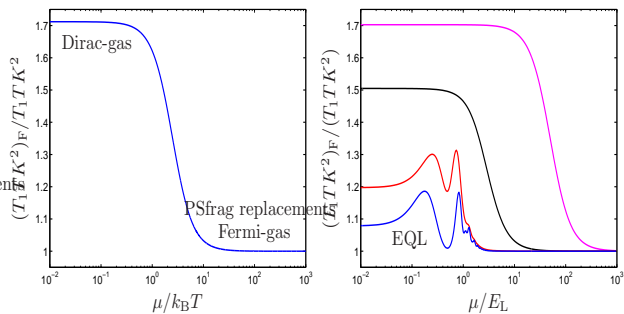


FIG. 2: (Color online) The Korringa relation, normalized to its Fermi-gas value, as function of $\mu/k_B T$ (left panel) and μ/E_L (right panel). The usual Korringa relation is recovered for $\mu \gg k_B T$ but for increasing T the normalized Korringa relation increases and saturates to $\pi^2/3 \ln^2(4)$. The right panel shows the Korringa relation for $\Gamma = 0.1 E_L$, which allows the visibility of the lowest Landau levels. The temperature is varied as $k_B T/E_L = 0.05, 0.1, 1$ and 20 from bottom to top. For $k_B T \sim \Gamma$, separate peaks indicate the Landau level structure, and the curves cross over to the field-free scaling limit with increasing T .

its conventional value, which signals the nature of Dirac fermions. The crossover can be explored even away from the DP by fixing the chemical potential to a finite value, and sweeping the temperature. Right at the DP, impurities spoil the crossover and re-establish the Fermi-gas relation for $(k_B T, \mu) \ll \Gamma$.

The Korringa relation can be numerically evaluated in the presence of Landau levels (i.e. for scenario (ii)) using Eq. 12 and Fig. 2 shows the result. For small T and Γ , the oscillatory behavior due to Landau levels in the DOS characterizes the Korringa relation. When $(k_B T, \Gamma) > E_L$, the Landau levels are smeared and the magnetic field does not play an important role thus the scaling limit is restored.

In Fig. 3, we summarize our findings on the NMR properties in the form of a "phase diagram". The extreme quantum limit shows up only at low temperatures and small chemical potential, when the Landau level structure is visible. Larger Γ , i.e. presence of defects, favors the Fermi-gas region.

We finally comment on the feasibility of NMR experiments in graphene. NMR is known to have a low signal sensitivity albeit its tremendous utility. In graphene, the NMR active ^{13}C nuclei has a low abundance ($c = 1.1\%$) and a low gyromagnetic ratio, $\gamma(^{13}\text{C}) \approx \gamma(^1\text{H})/4$. NMR spectrometers are characterized by the limit of detection (LOD) parameter, i.e. the number of nuclei required for a signal-to-noise ratio of three in a single acquisition. State-of-the-art spectrometers [17] have $\text{LOD}_0 = 10^{12}/\sqrt{\text{Hz}}$ for ^1H spins with sample and detector at 300 K in a 14 T magnetic field ($\nu(^1\text{H}) = 600$ MHz). For a general case the LOD is [18]:

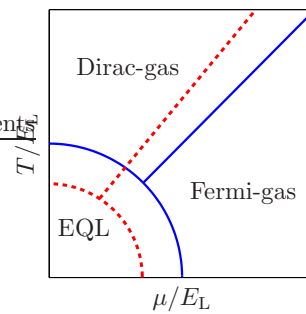


FIG. 3: The schematic "phase diagram" of graphene according to NMR, the phases are separated by solid lines. The boundaries denote smooth crossovers. The solid lines move to the dashed ones for increasing disorder.

$$\text{LOD} = \frac{\text{LOD}_0}{c} \sqrt{\frac{1 \text{ sec}}{T_2^*}} \left(\frac{\gamma(^1\text{H})}{\gamma} \right)^3 \frac{T_s}{300 \text{ K}} \text{NF}_{\text{rel}} \quad (15)$$

Here T_2^* is the apparent decay time of the NMR time-domain signal which contains the spin-spin relaxation time, T_2 , and the magnetic field inhomogeneity due to defects and the magnet. The Curie T dependence of the NMR signal is described by the sample temperature, T_s . NF_{rel} is the receiver noise factor relative to a receiver at 300 K.

Clearly, low sample temperature, low detector noise, and highly ^{13}C enriched graphene are required for an NMR study. Sample temperature down to 1 K is customary in solid state NMR and $\text{NF}_{\text{rel}} = 1/8$ was reported for cryo-probe NMR [19]. We estimate from NMR data on graphitic carbon [16, 20] that the $\text{FWHM} = 1/\pi T_2^*$ is 50 ppm at 14 T of fully ^{13}C enriched graphene giving $T_2^* = 10 \mu\text{s}$. This estimate assumes either a single graphene sheet or a set of graphene layers oriented alike. These factors give an LOD for ^{13}C graphene of $8 \cdot 10^{12}$ which corresponds to a surface of 0.63 mm^2 . We think that synthesis of a fully ^{13}C isotope enriched graphene with such an area (not necessarily of a single piece) is within reach as fully ^{13}C enriched graphite was recently synthesized [20]. We expect that a dedicated NMR microcoil setup, prepared by lithographic methods [17] would further decrease the LOD value and the required graphene sheet area.

In summary, we generalized the canonical theory of hyperfine interaction between nucleus and conduction electrons for graphene. The orbital part of the HFI differs from its usual form as it does not involve the angular momentum. We identified three distinct regimes in graphene based on the NMR measurables: Fermi- and Dirac-gas phases, and the extreme quantum limit. We argue that NMR on graphene is within realistic reach.

We acknowledge useful discussions with P. Thalmeier, A. Ványolos and T. Ma. Work supported by the Hungarian Scientific Research Fund under grants OTKA K72613

and F61733. F. S. acknowledges the Bolyai programme of the Hungarian Academy of Sciences.

-
- [1] C. P. Slichter, *Principles of Magnetic Resonance* (Spinger-Verlag, New York, 1989), 3rd ed.
- [2] N. A. Gershenfeld and I. L. Chuang, *Science* **275**, 350 (1997).
- [3] I. L. Chuang, L. M. K. Vandersypen, X. L. Zhou, D. W. Leung, and S. Lloyd, *Nature* **393**, 143 (1998).
- [4] L. C. Hebel and C. P. Slichter, *Phys. Rev.* **113**, 1504 (1959).
- [5] A. Abragam, *Principles of Nuclear Magnetism* (Clarendon Press, Oxford, 1961).
- [6] K. S. Novoselov, A. K. Geim, S. V. Morozov, D. Jiang, Y. Zhang, S. V. Dubonos, I. V. Grigorieva, and A. A. Firsov, *Science* **306**, 666 (2004).
- [7] A. H. Castro Neto, F. Guinea, N. M. Peres, K. S. Novoselov, and A. K. Geim, *Rev. Mod. Phys.* **81**, 109 (2009).
- [8] P. Lee and N. Nagaosa, *Phys. Rev. B* **43**, 1223 (1991).
- [9] J. J. van der Klink and H. P. Brom, *Prog. in Nucl. Magn. Res. Spec.* **36**, 89 (2000).
- [10] J. Cserti and Gy. Dávid, *Phys. Rev. B* **74**, 172305 (2006).
- [11] O. V. Yazyev, *Nano Lett.* **8**, 1011 (2008).
- [12] N. Sato, H. Tou, Y. Maniwa, K. Kikuchi, S. Suzuki, Y. Achiba, M. Kosaka, and K. Tanigaki, *Phys. Rev. B* **58**, 12433 (1998).
- [13] J. Winter, *Magnetic Resonance in Metals* (Clarendon Press, Oxford, 1971).
- [14] T. Moriya, *Prog. Theor. Phys.* **28**, 371 (1962).
- [15] S. G. Sharapov, V. P. Gusynin, and H. Beck, *Phys. Rev. B* **69**, 075104 (2004).
- [16] M. S. Dresselhaus and G. Dresselhaus, *Advances in Physics* **51**(1), 1 (2002).
- [17] P. J. M. van Bentum, J. W. G. Janssen, A. P. M. Kentgens, J. Bart, and J. G. E. Gardeniers, *J. Magn. Res.* **189**, 104 (2007).
- [18] C. Massin, F. Vincent, A. Homsy, K. Ehrmann, G. Boero, P. A. Besse, A. Daridon, E. Verpoorte, N. F. de Rooij, and R. S. Popovic, *J. Magn. Res.* **164**, 242 (2003).
- [19] P. Styles, N. Soffe, C. Scott, D. Cragg, D. White, and P. White, *J. Magn. Reson.* **60**, 397 (1984).
- [20] W. Cai, R. D. Piner, F. J. Stadermann, S. Park, M. A. Shaibat, Y. Ishii, D. Yang, A. Velamakanni, S. J. An, M. Stoller, J. An, D. Chen, *et al.*, *Science* **321**, 1815 (2008).
- [21] V. P. Antropov, I. I. Mazin, O. K. Andersen, A. I. Liechtenstein, and O. Jepsen, *Phys. Rev. B* **47**, 12373 (1993).
- [22] It is shown in Ref. [21] that neither dipolar nor orbital anisotropy affects the Korringa relation